This is the peer reviewed version of: Lees J.M. and Burgoyne C.J. (2000) "Analysis of concrete beams with partially bonded composite reinforcement" ACI Structural Journal V. 97(2) pp. 252-258.

Analysis of Concrete Beams with Partially-Bonded Composite Reinforcement

by J.M. Lees, C.J. Burgoyne

SYNOPSIS

Beams prestressed with partially-bonded fibre reinforced plastic (FRP) tendons have high strength and high rotation capacity, but cannot be modelled by conventional techniques. Here, it is assumed that all deformation takes place at cracks between rigid bodies. By setting up appropriate compatibility and equilibrium equations, the behaviour at a single crack can be modelled, which then allows predictions to be made as to which of four possible events will occur next. These lead, either to beam failure, or to changes in the geometry which can be analysed using the same techniques. Comparisons are made with test results and reasonable agreement is shown.

Key words : rigid body analysis, prestressed concrete, bond, flexure, advanced composites, aramid, FRP, fibre reinforced plastics

INTRODUCTION

Beams prestressed with FRP rods behave in a different way from beams with steel. The tendons do not exhibit plasticity, but have high strain capacity. If tendons are fully bonded they will tend to snap at the maximum load, while if unbonded, high moment capacity will not be achieved and the tendons will be used inefficiently.

To overcome these problems, it was proposed that beams should be made with partially-bonded tendons.[1] This can be achieved either by having alternately bonded and unbonded regions, or by coating the tendons with a resin of known, low, shear strength. The results of an experimental study have already been published by ACI[2], in which it was shown that moment capacities as good as those with bonded tendons could be achieved, but with rotation capacities in excess of those achievable with unbonded tendons.

However, the problem remains that a method of analysis is required. A conventional analysis, based on strain compatibility and plane sections remaining plane, is not valid as the tendon can move relative to the adjacent concrete. Nor do the methods used to analyse unbonded tendons work since the movement of the tendon is restrained. Thus, a more rigorous analysis is presented here. It is compared with experimental results for beams with aramid fibre tendons but the principles are more generally applicable and could be used as the basis of a design method.

RESEARCH SIGNIFICANCE

Because FRPs do not yield, a large rotation capacity is desirable for FRP-prestressed concrete beams. Furthermore, since FRPs are generally more expensive than steel it

will be important that they are used efficiently.

Conventional design methods do not give optimal results for FRP-prestressed structures and the use of partially-bonded tendons represents a more rational design basis for these novel materials.

This paper provides an analytical basis which can be used to predict the performance of beams with partially-bonded FRP tendons. The analysis highlights key events and design parameters which dictate the behaviour of these novel members.

EXPERIMENTAL STUDY

In the experimental study[2], pre-tensioned concrete beams with either fully-bonded, unbonded or partially-bonded FRP tendons were tested. The partial bonding was achieved in one of three ways, as shown in Figure 1. Intermittently-bonded (IB) tendons were made by alternately bonding and debonding lengths of tendon. In the IB-series 1 beams, the bonded lengths were very short and were designed to slip before the beam failed; in the IB-series 2 beams, the bonded lengths were designed not to fail. Adhesively bonded beams were made by coating the tendon, away from the anchorage zone, in a resin of low shear strength. Fully-bonded and unbonded beams were also tested but are not described here.

The beams were 2800mm$\times$200mm$\times$100mm and had either three 3.7 mm Fibra tendons or two 4 mm Technora tendons, both of which are made from aramid fibres (see Table 1). The tendons were pre-tensioned to approximately 65% of the tendon failure load. The beams were loaded in 4-point bending; the clear span was 2400mm and the constant moment region was 800 mm long.

ANALYSIS BASED ON STRAIN COMPATIBILITY

The behaviour up to first cracking can be modelled by a conventional strain compatibility approach, which also works up to failure for fully-bonded beams. However, for the partially-bonded beams after cracking, the beam is modelled by assuming that it behaves as a series of rigid blocks, which matches the experimental observation that most of the rotation takes place at a relatively small number of crack locations (Figure 2). Thus, the aim is to set up the relevant equilibrium and compatibility conditions at each crack. The process will be described in detail for a single crack - extension to multiple cracks is then straightforward.

Mathematical basis for rigid body analysis with a single crack

In Figure 3 the beam behaviour is modelled as two rigid blocks connected at a crack location, 1. The deflection of the beam at the crack location, δ_{cr1}, represents the movement relative to the original horizontal profile of the beam.

At the crack opening, the rotation is deemed to occur about the neutral axis which is at a depth nd. The concrete above the neutral axis is in compression and the extensions in the tendon are compatible with the crack opening. The total extension due to this rotation, δL_θ, is:

$$\delta L_\theta \quad = \quad \delta L_{\theta 1} + \delta L_{\theta 2} = 2d(1-n)\sin\left(\frac{\theta_1 + \theta_2}{2}\right) \tag{1}$$

The components of the tendon force in the x and y directions (which rotate with the blocks), F_{tx} and F_{ty}, are related to F, which is the force in the section of tendon

which spans the crack (see Equations 2 and 3).

$$F_{tx} = F \cos\left(\frac{\theta_1 + \theta_2}{2}\right) \quad (2)$$

$$F_{ty} = F \sin\left(\frac{\theta_1 + \theta_2}{2}\right) \quad (3)$$

The distribution of the force in the concrete compressive zone can be approximated as a rectangular stress block[8] (see Figure 4) as the concrete approaches its ultimate limit state. Immediately after cracking the concrete is likely still to be elastic and hence this type of plastic stress distribution is not appropriate. However, with further loading and with the onset of large strains, this model is reasonable.

The force in the concrete, F_{cx} is then given by

$$F_{cx} = (0.67 f_{cu})\ b\ (0.9nd) \quad (4)$$

Axial equilibrium requires:

$$F_{tx} = F_{cx} \quad (5)$$

If the force F_{tx} is known, the tendon extensions, δL_{Fx1} and δL_{Fx2}, due to the increase in the force in the tendon relative to the initial prestress level, $F_{tx} - P_o$, can then be calculated by considering the debonded lengths over which the tendon is free to extend, L_{db1} and L_{db2} (see Figure 3).

The sum of these extensions, δL_F, (Equation 6) can be equated to the extensions

predicted using Equation 1.

$$\delta L_F = (\delta L_{Fx1} + \delta L_{Fx2}) \cos\left(\frac{\theta_1 + \theta_2}{2}\right) = \frac{(F_{tx} - P_o)}{E_t A_t}(L_{db1} + L_{db2}) \cos\left(\frac{\theta_1 + \theta_2}{2}\right) \quad (6)$$

It is of note that for small rotations the cosine terms in Equations 2 and 6 will be approximately equal to 1.

Numerical procedure

Using the equations and assumptions of the previous section, a numerical procedure can be formulated to calculate the deflection profile of a beam for a given loading. The two primary variables are chosen to be the deflection at the crack location, δ_{cr1}, and the depth of the neutral axis, nd.

If the crack location, and hence the distances x_1 and x_2, are known, then for any particular value of δ_{cr1} the angles θ_1 and θ_2 are determinate.

The procedure can be summarised as follows:

- assume value of δ_{cr1}
- find θ_1 and θ_2
- iterate nd until $\delta L_F = \delta L_\theta$
- determine applied moment and loads
- repeat with new value of δ_{cr1}

Possible next events

The starting point for the rigid body analysis is that the first central crack has already occurred. After first cracking, the load is increased until one of several things happens:

1. The concrete will crush if the angle of rotation at the hinge location becomes excessive. A large rotation induces high localised strains in the concrete and results in the failure of the concrete.

2. The tendons will rupture if the strain in the tendon is greater than the extension capacity of the AFRP.

3. The bond in a segment will break down if the forces to be transmitted through the segment exceed the bond capacity of the region.

4. Another crack will form if the tensile stress build-up along the bottom face of the beam exceeds the tensile capacity of the concrete.

The occurrence of either event 1 or event 2 will result in the failure of the beam. However, events 3 and 4 can occur at various stages of loading.

Bond breakdown

Detailed models have been proposed to describe the bond stress-slip behaviour of reinforcement being pulled out of a block of concrete. In particular, the Comité Euro-International du Béton (CEB) Model Code[9] suggests that the variation of bond stress with slip can be described using a curve which consists of four parts (as shown in Figure 5). Note that the CEB model is based on the pull-out behaviour of steel reinforcement and the mechanisms involved are likely to differ when FRP rods are used.

However, others[10,11] have found that the model adequately describes the bond slip behaviour of some FRP rods.

In the present analysis, the treatment of bond is somewhat simplified (see Figure 5). In the ascending branch of the shear stress-displacement curve it is assumed that no slip occurs up to a maximum shear stress of τ_{max}. As the bond breaks down, the shear stress drops to τ_{frict}, remaining constant with increasing slip.

This simplified model is justified because large slips are expected in the current work. Hence the magnitude of slip that occurs prior to the bond breaking down will be small in comparison with the slip that will occur once only the frictional bond strength remains.

A further assumption is that the bond stress does not vary along the length of the bonded region. Hence $\tau = b_1$ where b_1 is a constant. As the bond stress is taken to be constant, the maximum force F_{max} that can be transmitted through the bonded region of length L_b prior to bond breaking down is the product of the maximum shear stress and the embedded surface area of the tendon.

$$F_{max} = 2\pi r L_b \tau_{max} \tag{7}$$

If the force to be carried by the bonded segment exceeds F_{max} then the bond breaks down and only a frictional bond resistance remains. Furthermore, large extensions occur through the region. As the shear stress, τ_{frict}, is assumed to stay constant with increasing displacements then the force transmitted through the bonded length, F_{frict},

does not vary, so that

$$F_{frict} = 2\pi r L_b \tau_{frict} \tag{8}$$

Generalised analysis procedure

For the intermittently-bonded beams a closed form solution for the force in terms of the deflection can be found. In the initial configuration the beam is subdivided into two halves with the centreline as the origin.

A schematic representation of how the forces in the tendon along the length of a beam can vary can be found in Figure 6. In this figure, the left hand side of a beam with a total of 23 segments is portrayed. Prior to loading, the force in the tendon segments is the initial prestress force P_o. However, as the applied load increases the forces in the tendon segments alter.

For the purposes of illustration, it will be assumed that for this particular combination of load, P, and rotation, θ_1, the bond in segments 9 and 11 has broken down and the frictional bond force is transmitted through these regions. The integrity of the bond in segment 7 is maintained (hence $T_8 - T_6 \leq F_{max}$) although bond forces are transmitted through the region.

For small rotations, the tendon forces in the unbonded segments on the left hand side of the beam can be calculated as follows:

$$\begin{aligned} T_{12} &= F \\ T_{10} &= T_{12} - F_{frict} \end{aligned}$$

$$T_8 = T_{10} - F_{frict}$$

$$T_6 = P_o$$

$$etc.$$

The force in the odd numbered segments T_{11}, T_9, T_7 etc. is taken to be the average of the force on either side of the segment under consideration.

In these equations, the frictional forces and the initial prestress are known. All the remaining forces along the length of the tendon can be found in terms of the force, T_{12}, in the centreline segment 12.

The overall extension of the tendon is then:

$$\delta L_F = \sum_{j=8}^{12} \frac{(T_j - P_o)L_j}{E_t A_t} \tag{9}$$

Further cracking - Build-up of stresses along bottom face

After first cracking has occurred, a knowledge of the build-up of stresses along the bottom face of the beam is necessary to ascertain where the next crack will form. To determine the stresses on the bottom surface a detailed analysis of the concrete is required; an analysis based solely on stress resultants is insufficient, since the local effects of the loads need to be considered. A beam model was formulated and both a theoretical analytical solution and a finite element solution were investigated.

Analysis model - Figure 7 shows the forces acting on the concrete in one half of a typical beam. These forces can be approximated by four separate loads acting on a

cantilever where the free end of the cantilever is analogous to the central crack face. The four loading components represent:

1. An eccentric point load normal to the end of a cantilever (to model the concrete compressive force).

2. A load acting at right angles to the top face of the cantilever (the applied load).

3. The combination of a vertical force applied at the tendon level and an equal and opposite force in the concrete compression zone applied at the end of the cantilever (to account for the vertical component of the tendon force, F_{ty}) (see Figure 3).

4. Internal point loads acting at the tendon depth (to simulate the bond forces applied to the concrete).

The fixed end of the cantilever does not reflect the actual support conditions, but this is not of concern since the applied loadings and internal forces will be in equilibrium. Superposition of the factored unit load case results will therefore result in a solution with no moment at the support. As there is no net moment at the left hand end, the effect of the clamped end in each of the individual analyses is, by St. Venant's principle, not significant near the far end of the cantilever when the four load cases are combined.

Theoretical analytical solution - Although it was known that a finite element analysis could be performed, an analytical solution would be preferable. However, exact solutions only exist for an eccentric point load[12,13] and they are extremely complex.

Finite element solution - An analysis using a finite element (FE) package was therefore carried out to determine the tensile stress build-up along the base of the beam.

It was found that the tensile stresses induced as a result of the vertical component of the tendon force (loading component 3) were small and have been neglected.

The finite element analysis showed that the most significant variations in stress at the bottom face were typically localised to within a region close to the point of the load application, as would be expected by St. Venant's principle. This effect was particularly noticeable in the concrete compressive force results.

The combined effect of the loading components on the tensile stress build-up will be determined in conjunction with the analysis at the crack. If the stress at a particular location along the length of the beam exceeds the tensile capacity of the concrete, a crack will occur.

Generalisation of formulation to multiple cracks

If further cracking occurs, the procedures outlined earlier can be generalised to consider the case where multiple cracks form under a given load condition (Figure 8). If the location of each new crack is known, then the deflection at the crack locations, δ_{cr}, is assumed. Using the assumed deflection profile, the neutral axis depth, nd, is then iterated until a solution is found which satisfies both the equilibrium and compatibility criteria (hereafter referred to as an equilibrium/compatibility solution). If no solution is found, then the assumed deflection profile is revised and the procedure repeated.

It is possible that there is more than one combination of deflection profile and neutral axis depth that would result in an equilibrium/compatibility solution; this should be considered for complex load histories.

If several cracks occur in a constant moment region, the force in the tendon spanning each crack must be the same. This feature was incorporated in the current analysis in

order to simplify the computation. In the majority of the experimental beams, the cracks did occur in the constant moment region and hence the assumption was valid. However, if this is not the case, refinements to allow for the varying compression and tension can be provided.

Additional repercussions of multiple cracking

- Bond stress direction

If a bonded region is located between two cracks then the region will be loaded from both directions; the behaviour depends on the bond state of the region prior to the occurrence of the second crack.[14]

- Tensile stress distribution

The build-up of concrete tensile stress along the bottom face of a block bounded by two cracks also changes. The resulting stress distribution depends on the length of the block, the force in the concrete and the status of any bonded segments within the block. In the results presented here it has been assumed that a further crack would not occur in such a block.

Computer program

A computer program was written to carry out the rigid body analysis. The input data includes the bond characteristics of the tendons and the details of the bonded and unbonded regions. Data files for the unit load cases, which correspond to the build-up of tensile stresses along the bottom face of the beam, are generated using the finite element program. The program calculates the first cracking moment using a strain-compatibility approach and then the iterative calculations commence.

The debonded length, L_{db}, reflects the distance between the outermost segments in which the bond has not broken down. For a set debonded length, the angle between the rigid blocks, θ, is incremented between the limits θ_{min} and θ_{max}; for each value of θ, the neutral axis depth, nd, is also incremented. The forces in the tendon and the concrete are calculated and checked for both axial force and moment equilibrium.

If an equilibrium/compatibility solution does not exist then θ is incremented and the process repeated. Conversely, when a solution has been found, the forces along the tendon are updated. The force in the tendon at the beam centreline is known from the previous step and hence the forces along the tendon can be calculated.

If the force in the tendon, T, is found to be equal to the failure load, P_{ult}, then tendon rupture occurs and the program is terminated. Otherwise, the forces transmitted through the bonded lengths are checked. If the forces exceed the bond capacity of a region, the bond is deemed to have broken down. If this is the case then L_{db} is increased and the loop repeated.

If the bond does not break down, the tensile stresses along the bottom face of the beam are checked to see if cracking occurs. If a crack does form, the status of the bond in the adjacent bonded regions and the forces in the tendon lengths next to the crack locations are adjusted and the process of checking for an equilibrium/compatibility solution, bond breakdown and cracking is repeated.

DISCUSSION

A comparison was made between the analytical and experimental results. The results for an intermittently-bonded FiBRA beam from series 1, an intermittently-

bonded Technora beam from series 2, an adhesive bonded FiBRA beam are presented below.

Input parameters

The input values for the bond parameters τ_{max} and τ_{frict} for both the adhesive-coated and uncoated tendons[14,15] are shown in Table 2. The concrete compressive cube and tensile modulus of rupture strength were approximately 56 MPa and 3.3 MPa respectively.

Intermittently bonded - Series 1

This series of beams was designed so that the load would break down as the load increased. A graph of the relationship between the applied load and rotation can be found in Figure 9. Bond breakdown and concrete cracking events are noted.

Both the experimental and predicted crack locations can be found in Table 3. The predicted tensile stresses along the bottom face of the beam often showed little variation near the maximum so a range of locations have been included in the table.

In general, the correlation between the experimental and analytical results for the first series of intermittently-bonded beams was quite good. The second and third crack locations were within the predicted range (see Table 3). However, the slopes of the predicted load vs θ curves are slightly lower than the experimental curves. This is probably due to the analytical concrete model which ignores concrete elasticity after cracking.

Tendon rupture, based on the manufacturer's assured strength rather than measured strength, was expected in the beam at a rotation of approximately 0.12 radians (in tests

described elsewhere[16] the measured strength of the tendon was found to be 15% higher than the assured strength). In the experimental beam the concrete started to fail at a rotation between 0.12 and 0.13 radians.

Intermittently bonded - Series 2

This series of beams was designed so that bond breakdown would not occur. A typical comparison is shown in Figure 10.

The correlation between the experimental and analytical results is not as good as for the series 1 beams. The load and rotation at which second cracking occurred are in agreement with the experiments. However, for the third crack, the predicted rotation is greater than the experimental value and the cracking load was underestimated. The analytical model predicts that failure would occur due to tendon rupture. In the experimental beam, failure was due to a combination of concrete crushing and tendon rupture which appeared to occur simultaneously.

The series 2 beams are not as sensitive to the values of τ_{max}, τ_{frict} as the series 1 beams.

In the experiments, the third crack occurred at a higher load than the second crack. In theory, if the bond does not break down and the bonded and unbonded segments are symmetrical about the beam centreline, both cracks should occur at a similar load. The experimental crack locations are up to 120 mm outside the constant moment region which also contradicts the theoretical prediction. This is probably due to the extensive horizontal cracking on either side of the central crack location during testing. It is expected that horizontal cracking will affect not only the crack location but also the cracking load and the rotation at which cracking occurs.

If cracks occur outside the constant moment region then the forces in the tendon lengths spanning the cracks are not equal to the centreline tendon force, as assumed, so the program will underestimate the load at which a particular rotation will occur.

Adhesive bonded

In Figure 11, the theoretical and experimental results for an adhesive-bonded beam are compared. The length of the adhesive-bonded tendons was arbitrarily treated as a series of 100 mm bonded tendon segments and it is predicted that there is an extensive breakdown of bond throughout testing.

The slopes of the predicted curves coincide fairly well with the experimental results. According to the computer analysis, the beam should have failed due to tendon rupture at a load of close to 7000 N. The computer program predicts failure based on the manufacturers' assured loads, P_{ult}, for the tendons. If the ultimate load capacity of the tendons is taken to be the measured tendon strength then a tendon failure would not occur until approximately 8000 N as observed.

Extensions/limitations of the program

The program was written specifically to elucidate the behaviour of the experimental beams. However, this type of analysis could be extended to include more general applications: a more refined bond stress-slip relationship could be incorporated; multiple tendon layers could be treated more rigorously and the FE results could be non-dimensionalised and linearised so that specific FE runs would not be needed for each new structure.

Other additions would be to incorporate a concrete model which reflects the load

history and the transition from the elastic to the elasto-plastic to the fully plastic state. However, there is a question of how to translate the displacements in the concrete which are calculated from the rigid body geometry into actual concrete strains. In order to do so the length of the region of concrete over which the displacement occurs is required and this value is unknown.

A constraint within the program is the assumption that the cracks occur inside the constant moment region. As evident even in the work presented here, this assumption is not always valid. The evaluation of the tendon force at a crack location outside the constant moment region is not problematic. The difficulty lies in the determination of the angles between the blocks. If the bond has not broken down then certain inferences about the angles between the blocks can be made. However, if the bond does break down, the distribution of the angles remains indeterminate and a solution can only be found by iterating through possible deflection profiles.

CONCLUSIONS

A simplified analysis, based on rigid body rotations of blocks between cracks, which satisfies both equilibrium of forces and compatibility of geometry, has been shown to model reasonably accurately the post-cracking behaviour of partially-bonded beams, and to allow the prediction of both failure loads and corresponding rotations. It is suggested that this type of analysis could be used to produce design guidelines.

ACKNOWLEDGEMENTS

The authors are grateful for the support of Teijin Ltd and Mitsui Construction Co. Kevlar is a trade name of Du Pont, Technora of Teijin and FiBRA of Mitsui. One of

the authors (JML) was sponsored by the Natural Sciences and Engineering Research Council of Canada (NSERC) and is appreciative of NSERC's financial assistance.

NOTATION

b	beam width
b_1	constant
d	effective depth of beam
f_{cu}	concrete compressive cube strength
f'_t	tensile strength of concrete inferred from cylinder strength
j	segment reference number
k	crack number
nd	neutral axis depth
r	tendon radius
s_1, s_2, s_3	values of slip
x	distance from end of the specimen
A_t	area of tendon
E_t	modulus of elasticity of tendon
F	tendon force
F_c	concrete compressive force
F_{cx}	component of concrete force in x-direction
F_{frict}	frictional bond force that can be carried by a region
F_{max}	maximum force carried by bonded region
F_{tx}	component of tendon force in x-direction
F_{ty}	component of tendon force in y-direction

L_b	bonded segment length
L_{db}	debonded length of tendon
P	applied load
P_o	initial prestress force
P_{ult}	manufacturer's assured load for tendon
R_i	tendon bond forces
S_c, S_t	vertical forces transmitted to the concrete
T	force in tendon segment
V_f	volume fraction of fibres
δ_{cr}	deflection at a particular crack
δL_F	total tendon extension due to force F
δL_θ	total tendon extension due to rotation θ
θ	angle of rotation
$\theta_{min}, \theta_{max}$	rotation limits
τ	bond shear stress
τ_f, τ_{frict}	frictional bond stress
τ_m, τ_{max}	average maximum bond shear stress

References

[1] C. J. Burgoyne. Should FRP be bonded to concrete?. In A. Nanni and C. W. Dolan, editors, *Fiber-Reinforced-Plastic Reinforcement for Concrete Structures - International Symposium, SP-138*, pages 367–380. American Concrete Institute, March 1993.

[2] J. M. Lees and C. J. Burgoyne. Experimental study of the influence of bond on the flexural behaviour of concrete beams pre-tensioned with AFRPs. *American Concrete Institute Structural Journal*, 96(3), May–June 1999.

[3] H. Mera and T. Takata. High performance fibers, *Ullmann's Encyclopedia of Industrial Chemistry*, volume A 13. VCH, 5th edition, 1989.

[4] Teijin Ltd. *High Tenacity Aramid Fibre - Technora.* Technical Information - TIE-05/89.11, 1989.

[5] T. Tamura. FiBRA. In A. Nanni, editor, *Fiber-Reinforced-Plastic (FRP) Reinforcement for Concrete Structures: Properties and Applications*, Developments in Civil Engineering, 42, pages 291–303. Elsevier Science Publishers B.V., 1993.

[6] M. Tanigaki, T. Okamoto, T. Tamura, S. Matsubara, and S. Nomura. Study of braided aramid fiber rods for reinforcing concrete. *IABSE, 13th Conference, Helsinki*, pages 15–20, 1988.

[7] R. Kakihara, M. Kamiyoshi, S. Kumagai, and K. Noritake. A new aramid rod for the reinforcement of prestressed concrete structures. In *Advanced Composites*

Materials in Civil Engineering Structures Proceedings, Las Vegas, Jan. 31, 1991, pages 132–142. MT Div/ASCE, Jan. 31 1991.

[8] E. Hognestad, N. W. Hanson, and D. McHenry. Concrete stress distribution in ultimate strength design. *Journal of the American Concrete Institute*, 27(4):455–479, December 1955.

[9] Comité Euro-International du Béton. *Bulletin D'Information No 203, CEB-FIP Model Code 1990 - Final Draft.* Chapters 1-3, July 1991.

[10] M. Faoro. The influence of stiffness and bond of FRP bars and tendons on the structural behaviour of reinforced concrete members. In M. M. El-Badry, editor, *Advanced Composite Materials in Bridges and Structures - 2nd International Conference*, pages 885–892. The Canadian Society for Civil Engineering, Montreal, Quebec, Canada, 11-14 August 1996.

[11] E. Cosenza, G. Manfredi, and R. Realfonzo. Bond characteristics and anchorage length of FRP rebars. In M. M. El-Badry, editor, *Advanced Composite Materials in Bridges and Structures - 2nd International Conference*, pages 909–916. The Canadian Society for Civil Engineering, Montreal, Quebec, Canada, 11-14 August 1996.

[12] G. Baker, M. N. Pavlović, and N. Tahan. An exact solution to the two-dimensional elasticity problem with rectangular boundaries under arbitrary edge forces. *Philosophical Transactions of the Royal Society of London*, 343(A):307–336, 1993.

[13] N. Tahan, M. N. Pavlović, and M. D. Kotsovos. Single fourier series solutions for rectangular plates under in-plane forces, with particular reference to the basic problem of colinear compression. Part 1: Closed-form solution and convergence study. *Thin-Walled Structures*, 15:291–303, 1993.

[14] J. M. Lees. *Flexure of Concrete Beams Pre-tensioned with Aramid FRPs*. PhD thesis, Department of Engineering, University of Cambridge, UK, 1997.

[15] S. Sheard. Bond characteristics and stress-slip model for aramid fibre reinforcement. Fourth Year Project, Department of Engineering, University of Cambridge, UK, May 1996.

[16] J. M. Lees, B. Gruffydd-Jones, and C. J. Burgoyne. Expansive cement couplers - A means of pre-tensioning fibre-reinforced plastic tendons. *Construction and Building Materials*, 9(6):413–423, 1995.

Biographical Sketches

Janet Lees completed her Ph.D. studies at the University of Cambridge, UK in 1997 and worked for a year as a post-doctoral researcher at the Swiss Federal Laboratories for Materials Testing and Research. She is currently working as a lecturer at the University of Cambridge, UK. Her research interests include the use of fibre reinforced plastics in construction applications and the behaviour of concrete structures.

Chris Burgoyne is a lecturer at the University of Cambridge, UK. He has been working with advanced composites applied to concrete structures since 1982. He is a member of ACI 440, and convenor of the Institution of Structural Engineers Study Group on Advanced Composites.

Table 1 : Tendon and fibre material properties[3,4,5,6,7]

Table 2 : Bond parameters used in analysis of beams

Table 3 : Crack locations for partially-bonded beams (distance in mms from left hand support)

Material	**Density** (kg/m^3)	**Fibre Type**	**Young's Modulus (GPa)**	**Max. Elong. (%)**	**Tensile Stren. (MPa)**	V_f (%)
FiBRA rod	1.28	Kevlar 49	68.6	2.0	1480	65-70
Kevlar 49 fibre	1.45	n/a	120.0	2.5	2800	n/a
Technora rod	1.3	Technora	54.0	3.7	1900	65
Technora fibre	1.39	n/a	73.0	4.6	3400	n/a
Steel (high yield)	7.8	n/a	200	10.0	650	n/a
Steel (prestress)	7.8	n/a	220	4.2*	1760	n/a

* measured value

Material	**Adhesive Coating**	τ_{max} **(MPa)**	τ_{frict} **(MPa)**
Technora	n	20	14
FiBRA	n	11	8
Technora	y	2.1	1.1
FiBRA	y	0.7	0.5

Beam Identification	**Experimental**		**Predicted**	
	crack 2	**crack 3**	**crack 2**	**crack 3**
Intermittently-bonded series 1	1560	830	1500-1600	800-900
Intermittently-bonded series 2	1720	730	1550-1650	750-850
Adhesive bonded	840	1550	840	1560

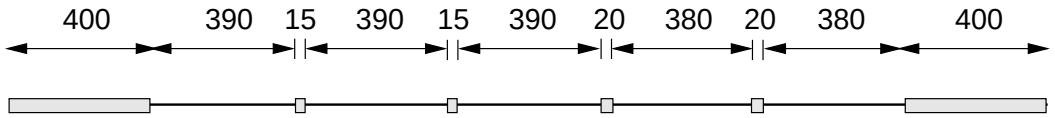

a) intermittently-bonded series 1

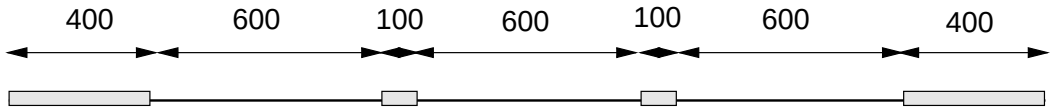

b) intermittently-bonded series 2

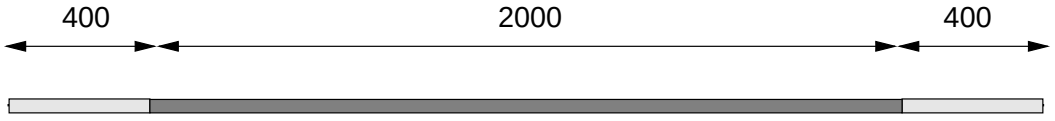

c) adhesive bonded

unbonded region

bonded region

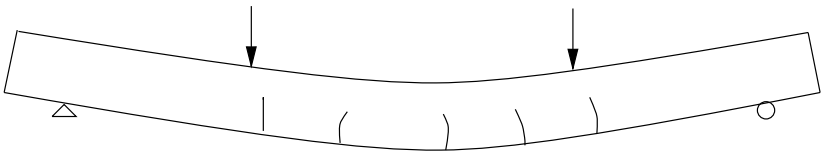

bonded analysis

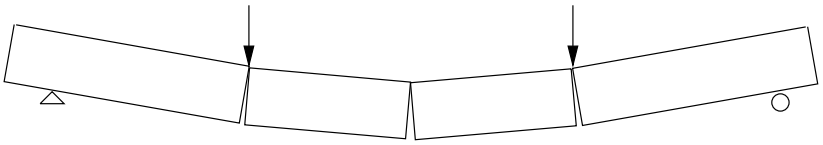

rigid block analysis

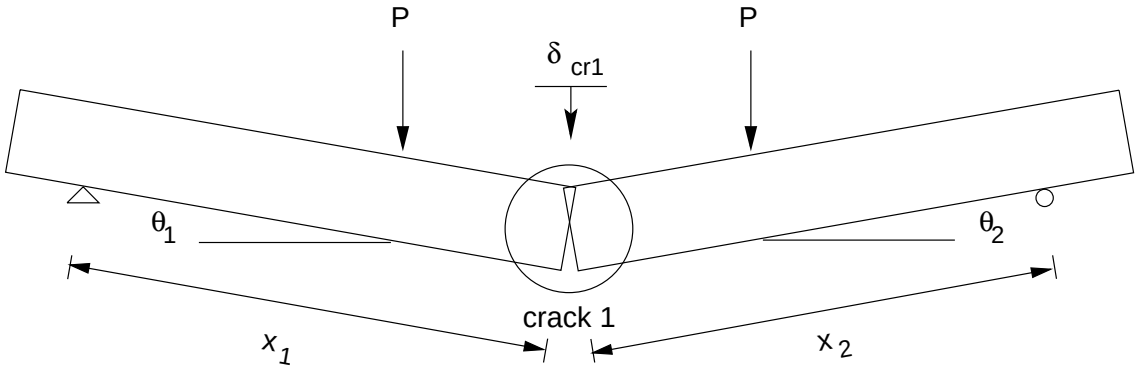
P
P
δ cr1
θ1
θ2
crack 1
x1
x2

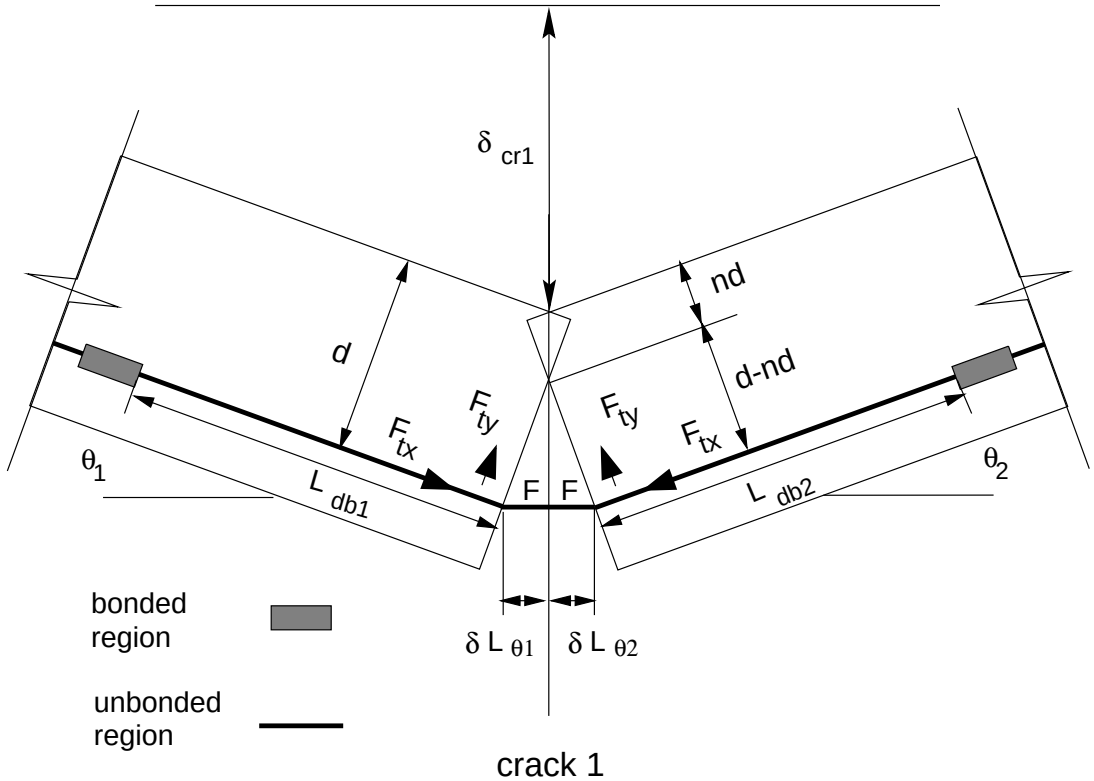
δ cr1
nd
d-nd
d
Ftx
Fty
Fty
Ftx
θ1
θ2
F F
Ldb1
Ldb2
δ Lθ1
δ Lθ2
bonded region
unbonded region

crack 1

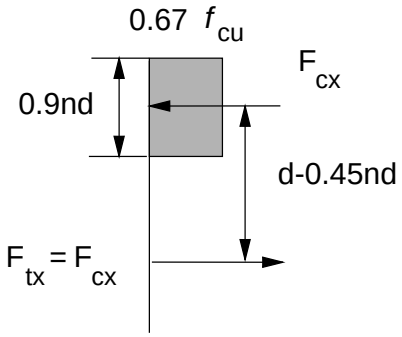
0.67 f_{cu}
F_{cx}
0.9nd
d-0.45nd
$F_{tx} = F_{cx}$

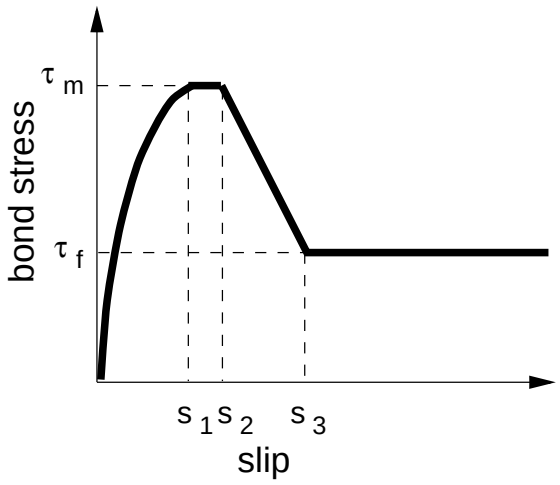

CEB Model Code

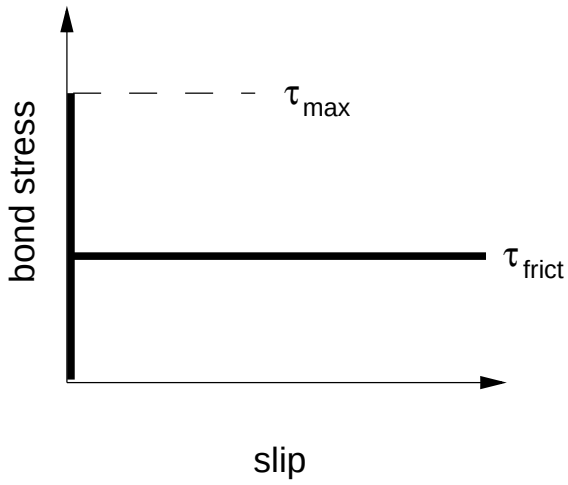

simplified model

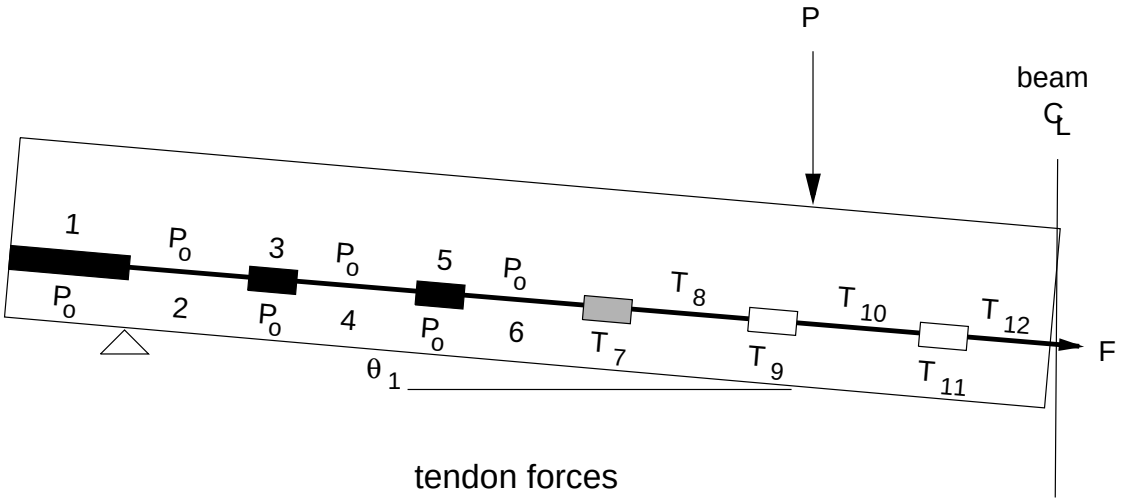

tendon forces

unbonded tendon

bonded region

fixed bond

frictional bond

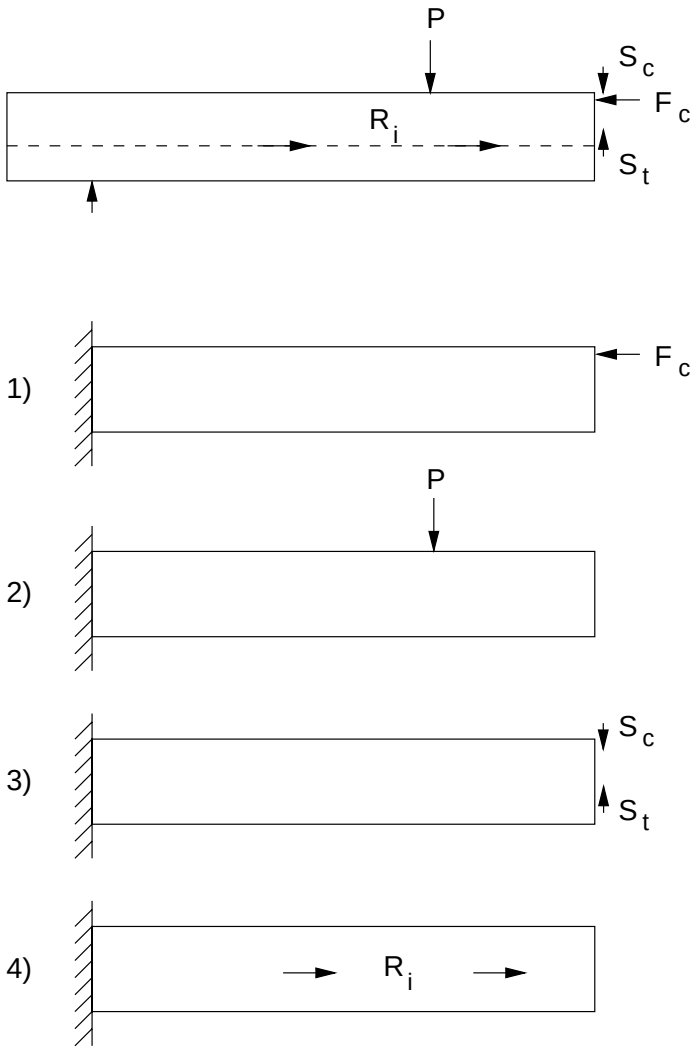
P
S c
F c
R i
S t
1)
F c
P
2)
3)
S c
S t
4)
R i

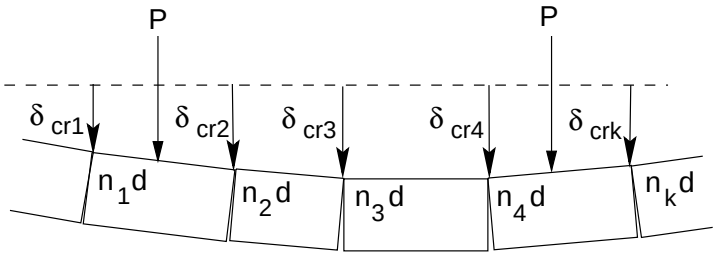
P
P
δ cr1
δ cr2
δ cr3
δ cr4
δ crk
n 1 d
n 2 d
n 3 d
n 4 d
n k d

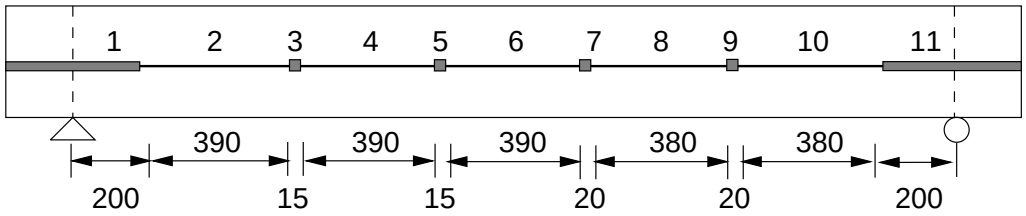
1
2
3
4
5
6
7
8
9
10
11
390
390
390
380
380
200
15
15
20
20
200

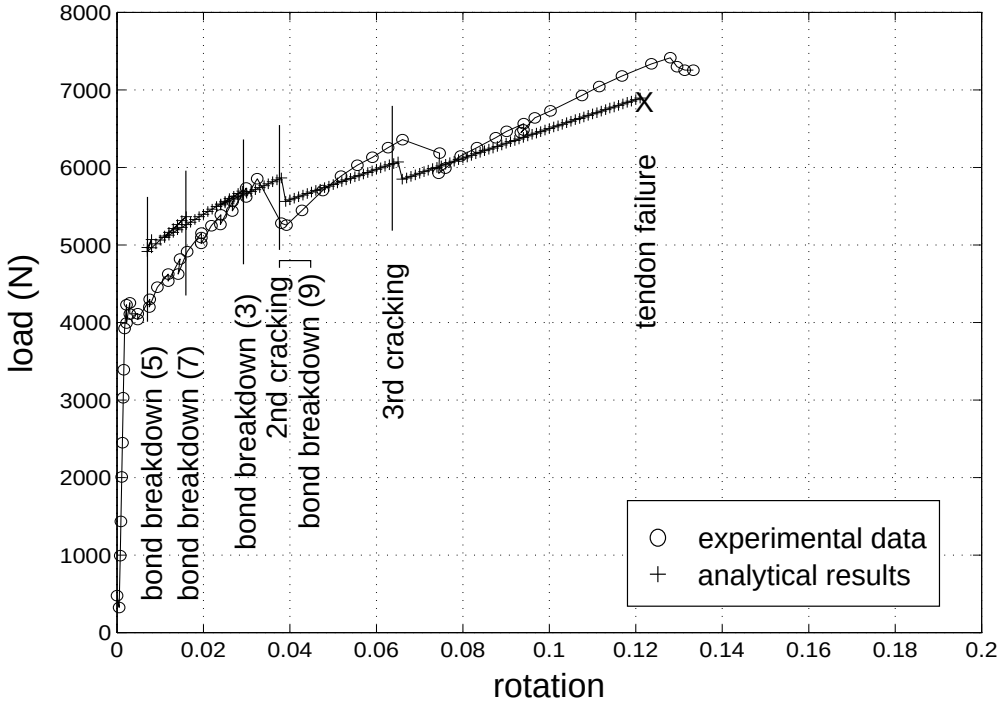
load (N)
rotation
bond breakdown (5)
bond breakdown (7)
bond breakdown (3)
2nd cracking
bond breakdown (9)
3rd cracking
tendon failure
experimental data
analytical results

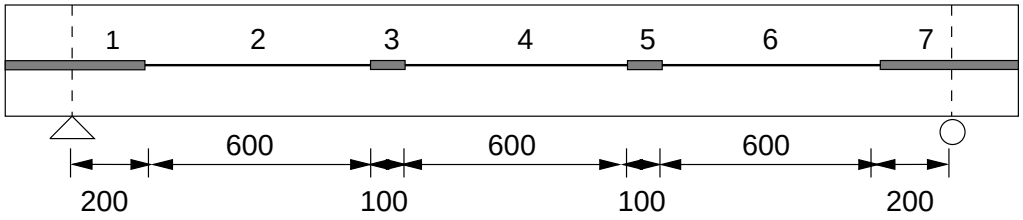
1
2
3
4
5
6
7
600
600
600
200
100
100
200

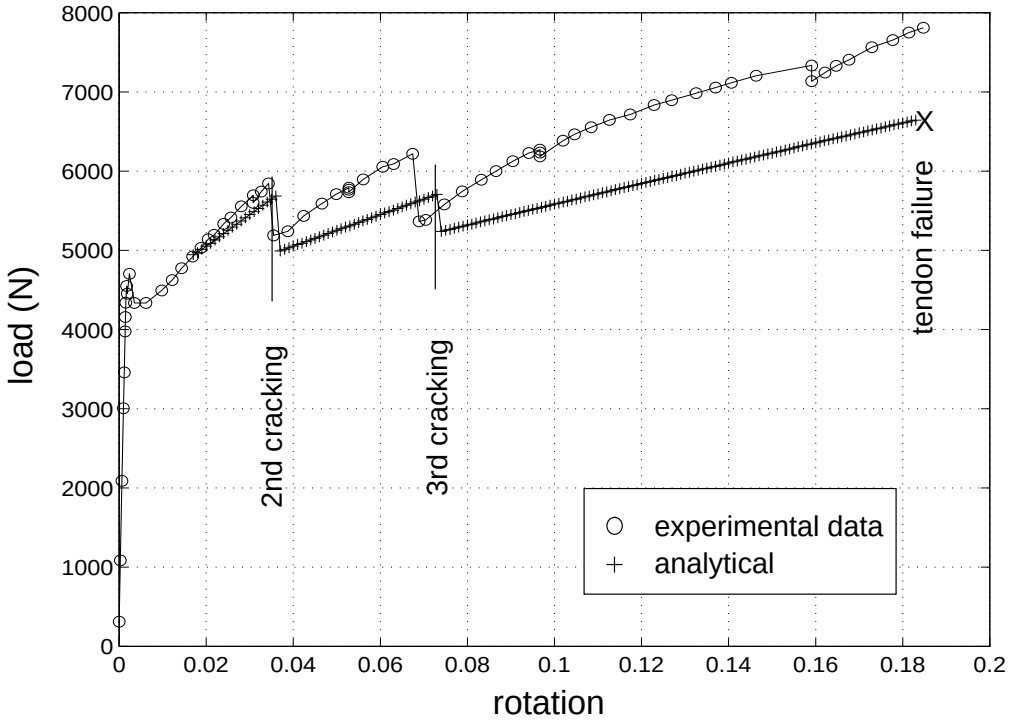
load (N)
rotation
2nd cracking
3rd cracking
tendon failure
experimental data
analytical
0
1000
2000
3000
4000
5000
6000
7000
8000
0.02
0.04
0.06
0.08
0.1
0.12
0.14
0.16
0.18
0.2

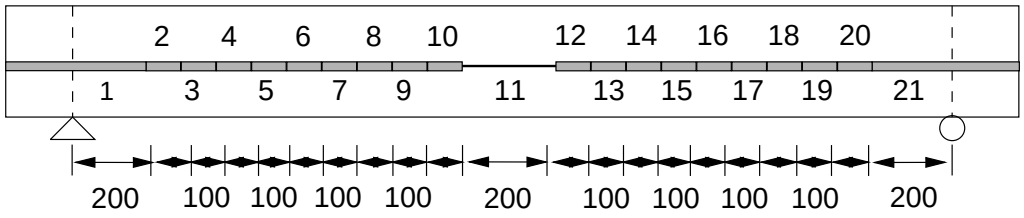
2 4 6 8 10 12 14 16 18 20
1 3 5 7 9 11 13 15 17 19 21
200 100 100 100 100 200 100 100 100 100 200

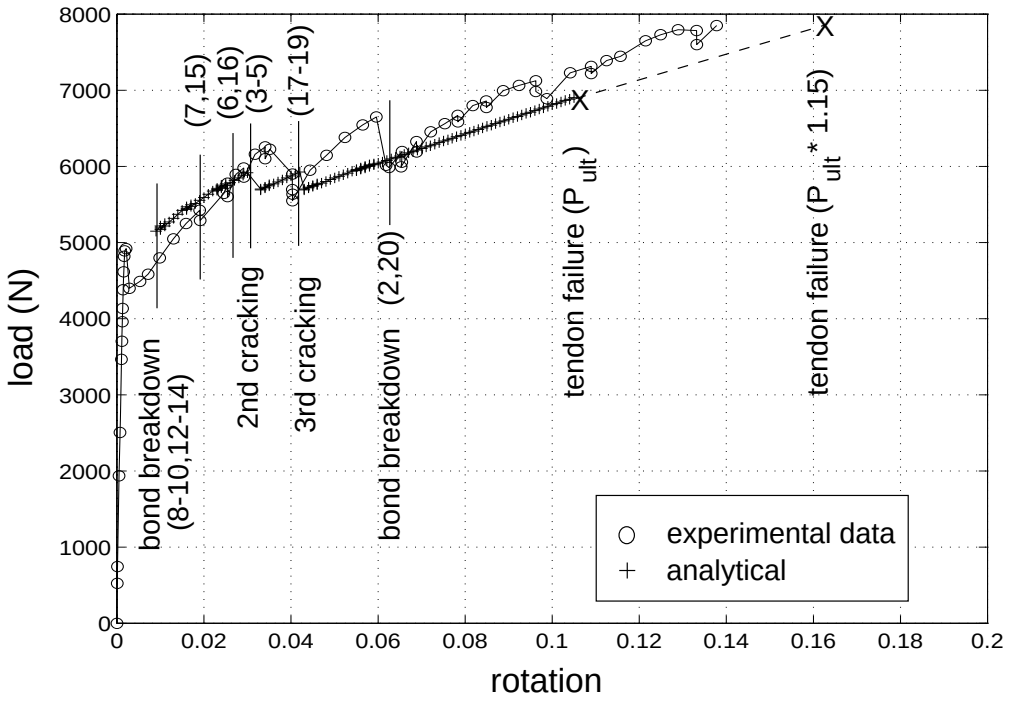
load (N)
rotation
0
1000
2000
3000
4000
5000
6000
7000
8000
0 0.02 0.04 0.06 0.08 0.1 0.12 0.14 0.16 0.18 0.2
(7,15)
(6,16)
(3-5)
(17-19)
bond breakdown (8-10,12-14)
2nd cracking
3rd cracking
bond breakdown (2,20)
tendon failure (P_ult)
tendon failure (P_ult * 1.15)
experimental data
analytical